High-resolution trace element records of an ice core from the eastern Tien Shan, central Asia, since 1953 AD

Yaping Liu,[1] Shugui Hou,[1,2] Sungmin Hong,[3,4] Soon Do Hur,[3] Khanghyun Lee,[3] and Yetang Wang[5]

Received 12 October 2010; revised 28 February 2011; accepted 4 April 2011; published 30 June 2011.

[1] High-resolution records of trace elements (Ba, V, Cr, Mn, Co, Ni, Cu, As, Rb, Sr, Mo, Cd, Sn, Sb, Tl, Pb, Bi, Th, and U) quantified in an ice core recovered from the Miaoergou glacier in the eastern Tien Shan, central Asia, spanning the period 1953–2004 AD, provide the first comprehensive time series on characterizing the relative contributions from natural and anthropogenic sources to the deposition of trace elements in central Asia. It is suggested that rock and soil dust is the most important natural source for most of elements investigated. Slight decreases in concentrations (or fallout fluxes) of crustal elements, such as Ba, Mn, Rb, Th, U, and Sr are observed during recent decades, which may be due to decreases in dust emissions from source regions and a decrease of accumulation rate since 1980s. The increasing trends of median concentrations and crustal enrichment factors (EF_c) of V, Cr, Co, Ni, Cu, and Mo, during the period 1953–2004 AD, are insignificant in comparison to their respective levels prior to 1953 AD. However, slight enhancements of both concentrations and EF_c are observed for Cd, Sb, Pb, Bi, Tl, and Sn since 1950s. Such recent increases are likely to be attributed to enhanced anthropogenic emissions, such as metal smelting, mining, stationary fossil fuel combustion, and combustion of gasoline due to human activities in Eurasia, particularly Xinjiang in northwestern China, Russia, and Kazakhstan. Our study supports evidence that environmental contamination has become a global problem for Pb and Bi and a large-scale phenomenon for Cd, Sb, Tl, and Sn.

Citation: Liu, Y., S. Hou, S. Hong, S. D. Hur, K. Lee, and Y. Wang (2011), High-resolution trace element records of an ice core from the eastern Tien Shan, central Asia, since 1953 AD, *J. Geophys. Res.*, *116*, D12307, doi:10.1029/2010JD015191.

1. Introduction

[2] Trace element pollution resulting from anthropogenic emissions is evident throughout most of the atmosphere and has the potential to create environmental and health risks [*Pacyna and Pacyna*, 2001]. Research undertaken into the occurrence of trace elements in snow and ice from Greenland, Antarctica, and high-altitude Andes, Himalayas, and European Alps has provided distinct evidence that atmospheric pollution of various trace elements exists on regional, hemispheric, and global scales, as a result of long-range transport and dispersion [*Boutron et al.*, 1995; *Planchon et al.*, 2002; *Barbante et al.*, 2004; *Hong et al.*, 2004, 2009; *Kaspari et al.*, 2009]. Many of these studies have also documented increasing concentrations for many trace elements in the 20th century but decreasing concentrations for certain trace elements (e.g., Pb, Cd, and Zn) during recent decades, due to the control of emissions in Europe and North America [*Boutron et al.*, 1995; *Van de Velde et al.*, 2000].

[3] The arid regions of central Asia contain some of the most extensive dust aerosol production areas in the world. Asian emissions are now the largest anthropogenic sources of atmospheric trace elements and still show an increasing trend [*Pacyna and Pacyna*, 2001]. Thus snow and ice records of trace elements from high-altitude alpine glaciers in central Asia are critical for a better understanding of changes in the relative contributions of natural and anthropogenic sources in this region. Previous data from central Asia have demonstrated increasing concentrations of trace elements, as a result of anthropogenic emissions, such as Bi, U, and Cs since 1950s [*Kaspari et al.*, 2009] and As, Mo, Sn, and Sb since 1970s [*Hong et al.*, 2009] in the Himalayas and Sb, Bi, and Pb from mid-1960s to 1990s in the Muztagh Ata [*Y. Li et al.*, 2006; *Z. Li et al.*, 2006].

[4] Tien Shan is located in a remote area of central Asia, surrounded by vast dust source areas (Figure 1). To the

[1]State Key Laboratory of Cryospheric Sciences, Cold and Arid Regions Environmental and Engineering Research Institute, Chinese Academy of Sciences, Lanzhou, China.
[2]MOE Key Laboratory for Coast and Island Development, School of Geographic and Oceanographic Sciences, Nanjing University, Nanjing, China.
[3]Korea Polar Research Institute, Incheon, South Korea.
[4]Department of Oceanography, Inha University, Incheon, South Korea.
[5]Shandong Marine Fisheries Research Institute, Yantai, China.

0148-0227/11/2010JD015191

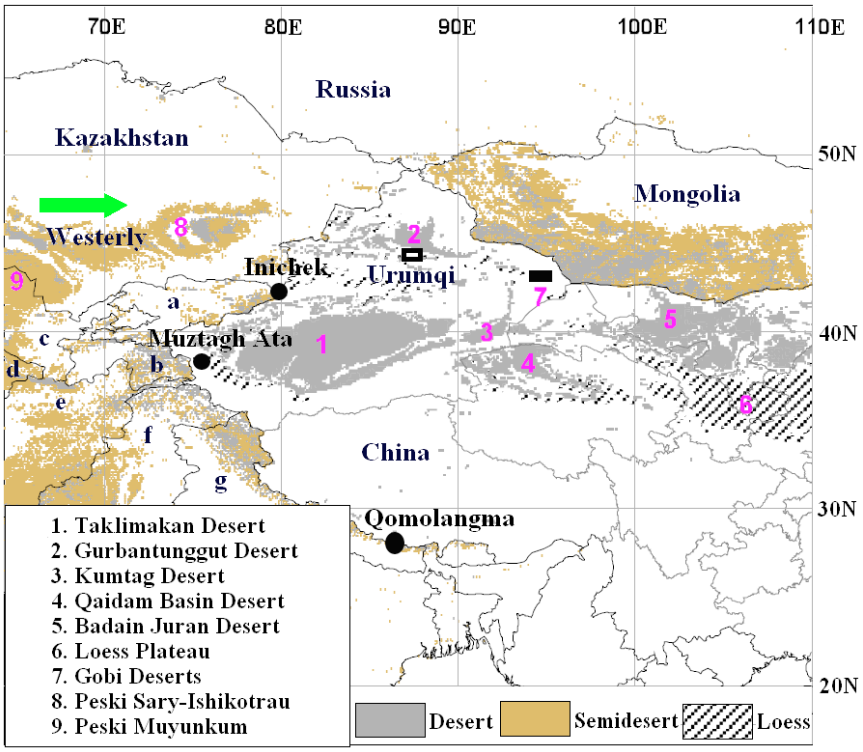

Figure 1. Location map of the Miaoergou ice core drilling site (solid black rectangle), other ice core sites mentioned in central Asia (solid black circles), and the surrounding dust sources (numbered) and countries: a, Kirghizstan; b, Tadzhikistan; c, Uzbekistan; d, Turkmenistan; e, Afghanistan; f, Pakistan; and g, India.

south lies the Taklimakan Desert; to the east are the Gobi Deserts, the Mongolian Gobi Plateau, and the Kumtag Desert; to the north is the Gurbantunggut Desert; and to the west are the Peski Muyunkum and the Peski Sary-Ishikotrau deserts. Moisture is primarily derived from the west and the north [*Wake et al.*, 1990, and references therein]. It is suggested that 87% of snow accumulation forms from precipitation originating from the Aral-Caspian closed basin, the eastern Mediterranean Sea, and the Black Sea and the remaining 13% originates from the North Atlantic [*Aizen et al.*, 2006]. Thus Tien Shan provides an ideal site for studying the long-range transport of atmospheric trace elements. However, previous research on the occurrence of trace elements in snow and ice from Tien Shan is limited. The available data [*Kreutz and Sholkovitz*, 2000; *Z. Li et al.*, 2007a] represent at a relatively short timescale (months to years) and do not provide sufficient consideration to anthropogenic sources. Therefore further studies on changes of trace elements during recent decades in Tien Shan are important for an improved understanding of the anthropogenic perturbation of atmospheric trace elements in this region. Since most of the previous determinations of trace elements in snow and ice were based upon discrete sampling method because of complicated decontamination procedures [e.g., *Candelone et al.*, 1994], the depth or temporal resolution of trace element records is limited for most of the available data. Under such circumstances, an improved decontamination method, leading to continuous and highly resolved records, is required to better characterize the changing patterns of trace elements on the timescales being assessed.

[5] Here, we present high-resolution records of trace elements (V, Cr, Mn, Co, Ni, Cu, As, Rb, Sr, Mo, Cd, Sn, Sb, Ba, Tl, Pb, Bi, Th, and U) along an ice core recovered from the eastern Tien Shan, central Asia, spanning the period 1953–2004 AD. The data were obtained by using an improved method for the decontamination of ice core samples. To our knowledge, the present work provides the first data for most of the trace element from the Tien Shan snow and ice. Our results expand the knowledge of the spatial and temporal variability of trace elements in snow and ice in the high-altitude Tien Shan region, identifying potential source areas.

2. Methods

2.1. Ice Core Sampling

[6] In 2005, two ice cores to bedrock (58.7 m and 57.6 m in length for Core 1 and Core 2, respectively) were recovered from a dome on the Miaoergou glacier (43°03′19″N, 94°19′21″E, 4512 m a.s.l.). There is no modern glacier to the east of the Miaoergou glacier in the eastern Tien Shan. The low borehole temperature at the drilling site (−7.2°C at 10 m depth and −8.2°C at the bottom, respectively) is beneficial for the preservation of ice core records. The ice cores were transported frozen to the State Key Laboratory of Cryospheric Sciences (SKLCS) for processing. This study is based upon the records obtained from Core 2. Core 2

Table 1. Detection Limit, Procedure Blank, and Analytical Results of Certified Reference Material SLRS-4[a]

Element	Mass Number	Detection Limit	Procedure Blank[b]	SLRS-4 (×1000)		
				Found	Certified	*Krachler et al.* [2005a]
V	51	2.7	4.8 ± 3.6	0.36 ± 0.004	0.32 ± 0.03	
Cr	53	21.4	74.4 ± 21.6	0.35 ± 0.02	0.33 ± 0.02	
Mn	55	1.5	20.3 ± 16.2	3.39 ± 0.03	3.37 ± 0.18	
Co	59	0.5	1.4 ± 0.6	0.041 ± 0.003	0.033 ± 0.006	
Ni	60	2.1	16.1 ± 13.9	0.78 ± 0.03	0.67 ± 0.08	
Cu	63	1.5	7.5 ± 4.8	1.83 ± 0.08	1.81 ± 0.08	
As	75	2.6	5.3 ± 1.6	0.72 ± 0.02	0.68 ± 0.06	
Rb	85	0.5	<D.L.	1.43 ± 0.05	—	1.40 ± 0.07
Sr	88	0.3	4.1 ± 1.2	28.3 ± 0.01	26.3 ± 3.2	
Mo	95	0.5	0.7 ± 0.3	0.20 ± 0.01	0.21 ± 0.02	
Cd	114	0.7	<D.L.	0.014 ± 0.001	0.012 ± 0.002	
Sn	118	1.2	3.8 ± 2.0	0.009 ± 0.001	—	
Sb	121	0.5	<D.L.	0.24 ± 0.003	0.23 ± 0.04	
Ba	138	0.8	7.0 ± 3.1	12.3 ± 0.1	12.2 ± 0.6	
Tl	205	0.1	0.2 ± 0.0	0.007 ± 0.001	—	0.0054 ± 0.0003
Pb	208	0.3	34.0 ± 30.3	0.083 ± 0.002	0.086 ± 0.007	
Bi	209	0.1	<D.L.	0.002 ± 0.001	—	0.0021 ± 0.0001
Th	232	0.1	0.2 ± 0.1	0.02 ± 0.001	—	
U	238	0.3	<D.L.	0.050 ± 0.001	0.050 ± 0.003	

[a]Unit of measure is pg g^{-1}.
[b]D.L. is detection limit.

(~9.4 cm in diameter) was split axially into two equal halves. One half was stored for archive purpose; the other was sampled continuously at intervals of ~4–5 cm in a cold room (−20°C). A total of 1205 sections were obtained for the measurements of trace elements, stable oxygen isotopes, major ions, and insoluble microparticles. The samples for stable oxygen isotopes were cut axially from both sides (~1 cm for each side) of each section. The ice core sections for trace element measurement, after decontamination as described below, were put in clean low-density polyethylene (LDPE) bags for further decontamination.

2.2. Decontamination of the Ice Core Sections

[7] The conventional decontamination technique for trace element measurement was developed for polar firn/ice cores. This technique includes progressively chiseling away the potentially contaminated outer portion of the cores, under clean conditions [e.g., *Candelone et al.*, 1994]. However, this method is only suitable for discrete samples with lower depth resolution (10–20 cm/sample) because it requires complicated decontamination procedures and large sample volumes. In this study, a custom designed lathe (constituted of polymethyl methacrylate) was used to decontaminate the ice core samples. The lathe was evolved from that used by *Candelone et al.* [1994] but with some geometric differences; these permit the short cores (~5 cm) to be retained vertically in the lathe. Stainless scalpels with replaceable blades and ceramic knives were used to remove the potential contamination from the outside portion, toward the inner core. The decontamination procedure was performed in a class 100 laminar flow clean bench, located inside a cold room at −12°C. Operators worked in coordination, wearing nonparticulating clean suits and using LDPE gloves, which were replaced frequently as required, depending upon the different degrees of cleanliness of various items. The cleaning of the polyethylene (PE) bottles, polypropylene (PP) tongs, and other laboratory equipment followed the successive acid cleaning procedures in SKLCS, as described by *Liu et al.* [2009].

[8] Each core section was handled in a series of steps. Initially, ~5 mm ice from both ends was shaved off, using a clean stainless scalpel. The core section was then placed in the lathe and the first ~5 mm thick veneer layer was shaved off, using a clean stainless scalpel. Afterwards, the operator changed LDPE gloves and a second veneer layer was shaved off, using a new clean stainless scalpel. This procedure was repeated and the third veneer layer was shaved off, using a clean ceramic knife. The remaining part of the core section was then held with homemade PP tong and ~5 mm ice from both core section ends was shaved off, using clean ceramic knives. Finally, the remaining inner core section was placed into a clean LDPE bag. The ice chips shaved off during decontamination were collected for measurements of β activity. Artificial ice cores were formed by freezing ultra-pure Milli-Q water in PFA Teflon cylinders, with a length of ~6 cm and a diameter of ~5 cm, respectively. A procedural blank of six samples (Table 1) was established by processing the artificial cores in a similar way as for the real ice cores.

[9] The removed layers from the outside to the inner core were collected from three core sections to verify if the inner parts of the core sections were free from outside contamination. The changes in the measured concentrations for Pb, Bi, Cd, and Cu, as a function of radius from the outside to the inside of the core, are shown in the auxiliary material (Figure S1).[1] It can be observed that the concentrations of elements decreased significantly from the external layers to the inner core. Although no well-established plateau values in the central parts of the sections were observed, this is probably due more to the inhomogeneity

[1]Auxiliary material data sets are available at ftp://ftp.agu.org/apend/jd/2010jd015191. Other auxiliary material files are in the HTML.

Table 2. Statistical Summary of Trace Element and Ca Concentrations for the Pre-1953 AD and Post-1953 AD Periods[a]

	Pre-1953				Post-1953					
Element	Min	Max	Mean	Median	Min	Max	Max/Min	Mean	SD[b]	Median
Ba	119	75213	6135	4357	311	48668	157	5622	5917	4047
V	33	24069	1342	931	58	13038	223	1369	1572	934
Cr	46	19704	1098	758	69	10607	154	1092	1289	734
Mn	276	505433	26063	17211	889	236479	266	22408	27066	15014
Co	1.7	8752	419	266	13	4857	384	402	534	247
Ni	27	20784	1094	738	33	12363	372	1080	1364	709
Cu	16	16919	992	699	52	11135	215	1061	1250	718
As	10	2905	350	298	12	2516	211	420	312	342
Rb	29	22614	1384	989	52	12421	240	1316	1490	878
Sr	654	132225	10676	8952	227	42603	188	8303	7337	5848
Mo	1.8	284	33	28	1.4	151	107	33	24	27
Cd	0.8	279	12	8	1.0	235	240	27	28	21
Sn	1.3	161	19	14	1.3	226	168	30	24	23
Sb	1.2	163	23	19	4.2	208	49	41	27	35
Tl	0.5	215	11	8	0.9	144	163	13	17	9
Pb	44	12628	783	528	30	19471	655	1652	1997	1147
Bi	0.4	149	11	9	0.6	176	299	19	22	13
Th	3.3	3081	179	122	3.4	1822	534	156	215	95
U	4.7	1095	84	61	4.2	624	150	70	74	50
Ca	96	14861	2345	2065	135	9989	74	1956	1702	1432

[a]Trace elements unit of measure is pg g^{-1} and Ca unite of measure is ng g^{-1}. Pre-1953 AD corresponds to 879 samples and post-1953 AD corresponds to 326 samples.
[b]SD means standard deviation.

of the core sections than to a possible contamination originating from the external layers.

2.3. Chemical Measurements

[10] The decontaminated inner core sections were melted at room temperature (~20°C), inside a class 100 clean bench in a class 10000 clean room in SKLCS. Two aliquots were then taken, for measurements of major ions and microparticles (15–20 mL) and trace elements (15–20 mL), respectively. On the basis of the higher concentrations of trace elements in the Miaoergou samples, effect resulting from absorption on the container might be insignificant. The samples for trace element measurements were acidified to 1% (a foregoing test suggested that this was an appropriate level for acidification of the Miaoergou snow samples [*Y. Li et al.*, 2007]), with Fisher "Optima" grade ultrapure HNO_3 and allowed to react with the acid for 7 days, then frozen until measurements were undertaken. Measurements of major ions, stable oxygen isotopes, microparticles, and β activity were performed in SKLCS. Major cations and anions were analyzed using a Dionex 600 and ICS-2500 ion chromatograph (with a detection limit of 1 ng g^{-1}), respectively, stable oxygen isotopic ratios using a Finnigan MAT-252 mass spectrometer (accuracy of 0.05‰), microparticles using an Accusizer 780 A Opitical Particle Sizer (Particle Sizing System, USA), and β activity using a MINI20 low background α/β counting system (CANBERRA EURISYS).

[11] Measurements of trace elements were performed in the Korea Polar Research Institute (KOPRI), using an Inductively Coupled Plasma Mass Spectrometer (ICP-MS) (Perkin Elmer Sciex, ELAN 6100). Detailed information on instrument settings and optimization was described by *Lee et al.* [2008]. Prior to measurements, the samples were melted at room temperature, inside a class 10 clean bench located in a class 1000 clean room. External calibration curves were used for quantification. The ICP-MS data were blank-corrected, by subtracting the procedure blank values (Table 1).

[12] Detection limits, defined as three times that of the standard deviation of 10 measurements of blank solution (1% Fisher "Opitima" grade HNO_3 water solution), are presented in Table 1. The accuracy of the method was verified by analyzing a riverine water reference (SLRS-4, River Water Reference Material for Trace Metals, National Research Council Canada, Ottawa, Canada). A good agreement between the measured and the certified values was observed for most of the measured elements (Table 1). The established Rb, Tl, and Bi values by *Krachler et al.* [2005a] are also listed in Table 1 for comparison purpose.

2.4. Ice Core Dating

[13] In central Asia, the first-order control on seasonal $\delta^{18}O$ variability is temperature [*Araguás-Araguás et al.*, 1998]. A high correlation between temperature and precipitation $\delta^{18}O$ was found for eastern Tien Shan [*Hou et al.*, 1999]. Accordingly, sections of lower $\delta^{18}O$ values along the core are interpreted as precipitation falling during cold winter seasons and those with higher $\delta^{18}O$ values, as precipitation falling during warm summer seasons.

[14] The crust species (e.g., Ca^{2+}, Ba^{2+}) in the eastern Tien Shan snow and ice show clear seasonal variability, i.e., higher concentrations during winter and spring due to strong dust input and lower concentrations during summer in response to heavy precipitation [*Z. Li et al.*, 2007a]. According to the seasonality of $\delta^{18}O$ and crustal species (Ca^{2+}, Ba^{2+}) (Table 2), the Miaoergou ice core was dated by counting annual layers. The dating result was verified further by the β activity horizons produced by global atmospheric thermonuclear tests in the Northern Hemisphere (1963 AD) and, possibly, at the nearby Lop Nur in western China during the period 1967–1970 AD (Figure 2). Core 2 was dated back to 1953 AD at 16.8 m depth (Figure 2), with an estimated dating uncertainty ±1 year for this period. The mean annual accumulation rate, calculated from the ice core dating result and density profile, is 26 g H_2O cm^{-2} yr^{-1} for

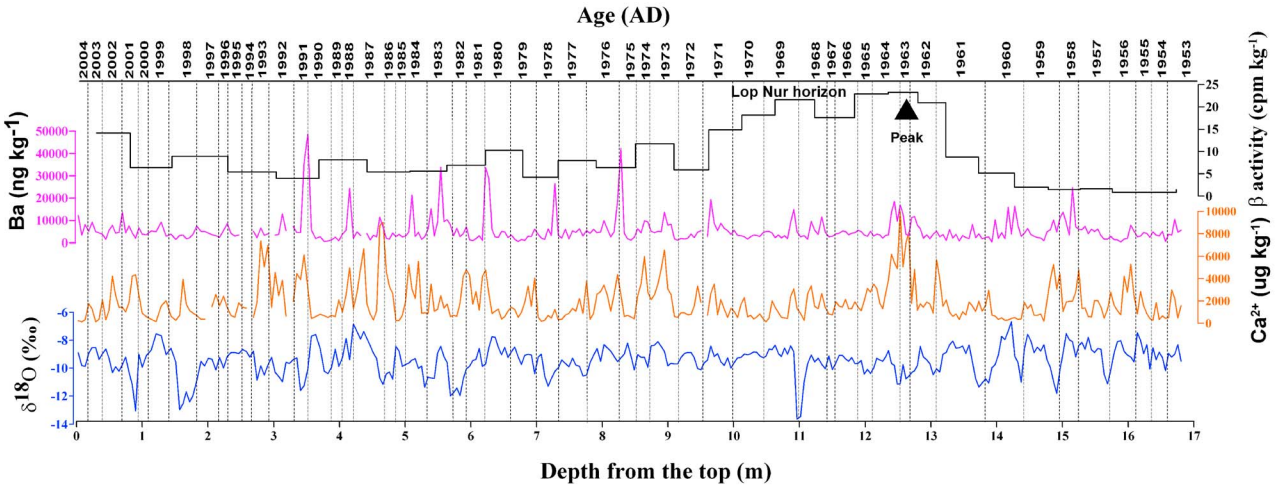

Figure 2. Dating of the Miaoergou ice core, on the basis of seasonal variation in calcium, barium, and $\delta^{18}O$. The results were verified by the β activity horizons produced by global atmospheric thermonuclear tests in the Northern Hemisphere (1963 AD) and, possibly, at the nearby Lop Nur in western China during the period 1967–1970 AD.

the period 1953–2004 AD. Interestingly, it has decreased significantly since 1980s, from 33 g H_2O cm^{-2} yr^{-1} during the period 1953–1979 AD to 20 g during recent decades. Although all 1205 samples were analyzed for trace elements and major ions, here we focus on the trace element data (326 samples) since 1953 AD because dating below 16.8 m is impossible by annual layer counting. In the future, a flow model and/or ^{210}Pb-dating will be applied for dating the whole Core 2.

3. Results and Discussion

3.1. Seasonal Variability

[15] To better facilitate readers to understand the results, data of trace elements and stable oxygen isotopic ratios ($\delta^{18}O$) since 1953 AD are presented in Data Set S1 in the auxiliary material. The statistics of the trace elements for the period 1953–2004 AD indicate that their concentrations differ by orders of magnitude, and there is large variability in the concentrations for each particular element (Table 2). The ratios of the maximum against the minimum concentrations range from 49 for Sb to 655 for Pb. Median values of trace elements vary from 9 pg g^{-1} for Tl to 15 ng g^{-1} for Mn (Table 2). These pronounced variations of element concentrations occur in relation to significant changes in the sources and transport of dust. The concentration peaks occur due to dust storm activities, associated with unstable atmospheric conditions and strong winds in the region during winter and spring. The low concentrations of trace elements may be caused by decreased dust flux, as well as heavy precipitation, which scavenges aerosols during summer.

3.2. Variations in Concentrations and Crustal Enrichment Factors

[16] Crustal enrichment factors (EF_c) can be used as indices to assess the relative contributions from crustal versus other sources. EF_c is defined as the ratio of the concentration of a given element to that of a conservative crustal element, normalized to the reference ratio of the upper continental crust [*Wedepohl*, 1995]. Using Ba as a crustal reference element, the calculation of EF_c for Pb is as $EF_c = (Pb/Ba)_{ice}/(Pb/Ba)_{crust}$. The primary uncertainty in these calculations may be attributed to the differences between chemical composition of local soil and reference crustal composition, as given by *Wedepohl* [1995]. If the calculated values of EF_c are approaching to unity, crustal contribution is suggested as a dominant source for the element. Conversely, if the EF_c values are larger than unity, contributions from other natural or anthropogenic sources become important.

[17] Figure 3 shows the changes in concentrations and EF_c of trace elements since 1953 AD, together with a five-point running mean to indicate their trends. The different trends of trace elements can be observed in spite of the influence of pronounced seasonal variations. To provide further evidence of long-term trends since 1953 AD and to investigate if anthropogenic activities are changing trace element loading of the atmosphere in the region, comparisons of recent changes with pre-industrial levels are necessary, because less anthropogenic inputs are expected during the preindustrial period. The age of the core sections below 50 m depth could be older than 1850 AD (preindustrial), assuming that the average precipitation rate did not change considerably during the past 200 years. Table 3 shows that the median concentrations of all (172) samples below 50 m to the bottom of Core 2 are similar to, or slightly higher than, the median concentrations pre-1953 AD (879 samples, from the depth 16.8 m to the bottom). This pattern indicates that anthropogenic inputs are limited in the high-altitude Tien Shan region, both pre-1953 AD and preindustrial periods. Thus the period pre-1953 AD (the statistics of the trace elements pre-1953 AD is presented in Table 2) is selected as a reference to facilitate comparisons between different periods since 1953 AD (Table 3). In this

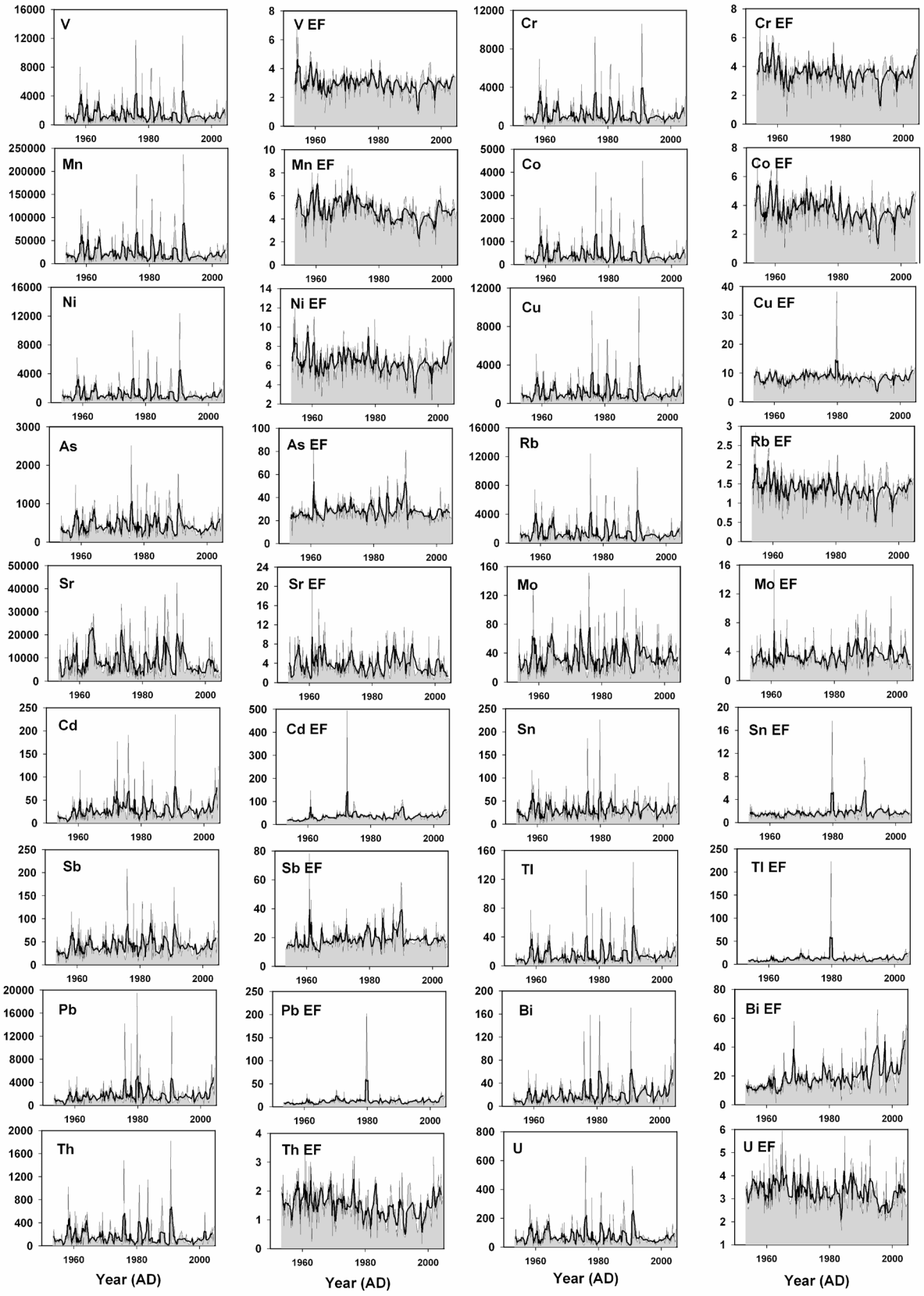

Figure 3. Concentrations (pg g^{-1}) and crustal enrichment factors (EF_c) of trace elements in the Miaoergou ice core from the eastern Tien Shan since 1953 AD. The solid lines show the five-point running mean trends.

Table 3. Trace Element Concentrations (pg g^{-1}), Crustal Enrichment Factors (EF) and Increase Factor (IF) for the Miaoergou Ice Core and the Data of Particle Number (10^3/mL) and Mass (ppb g^{-1}) Concentrations[a]

	Below 50 m Median	Pre-1953 Median	1953–2004 Median	1953–1959 Median	1960–1969 Median	1970–1979 Median	1980–1989 Median	1990–2004 Median	1953–2004 IF	1953–1959 IF	1960–1969 IF	1970–1979 IF	1980–1989 IF	1990–2004 IF
Ba	5013	4537	4047	4249	3800	4199	3550	4378	0.9	0.9	0.8	0.9	0.8	1.0
V	1064	931	934	1084	875	1040	797	931	1.0	1.2	0.9	1.1	0.9	1.0
Cr	919	758	734	919	681	783	597	772	1.0	1.2	0.9	1.0	0.8	1.0
Mn	19,954	17,211	15,014	17,474	15,081	17,593	11,294	13,703	0.9	1.0	0.9	1.0	0.7	0.8
Co	305	266	247	316	242	277	207	241	0.9	1.2	0.9	1.0	0.8	0.9
Ni	856	738	709	815	662	820	611	700	1.0	1.1	0.9	1.1	0.8	0.9
Cu	769	699	718	758	687	821	617	757	1.0	1.1	1.0	1.2	0.9	1.1
As	331	298	342	302	346	355	350	340	1.1	1.0	1.2	1.2	1.2	1.1
Rb	1124	989	878	1067	823	924	756	872	0.9	1.1	0.8	0.9	0.8	0.9
Sr	10,449	8952	5848	6100	6347	5281	5297	4672	0.7	0.7	0.7	0.6	0.6	0.5
Mo	33.3	28.1	26.8	24.4	28.5	23.7	29.5	28.5	1.0	0.9	1.0	0.8	1.0	1.0
Cd	8.0	7.8	21.1	12.4	21.2	25.6	19.5	24.6	2.7	1.6	2.7	3.3	2.5	3.2
Sn	16.2	14.7	23.0	21.2	22.2	21.6	23.8	28.2	1.6	1.4	1.5	1.5	1.6	1.9
Sb	20.7	19.2	35.3	27.9	34.3	36.5	40.7	37.0	1.8	1.5	1.8	1.9	2.1	1.9
Tl	8.6	7.5	8.9	8.3	7.6	8.1	7.4	11.7	1.2	1.1	1.0	1.1	1.0	1.6
Pb	529	528	1147	798	1183	1444	1110	1384	2.2	1.5	2.2	2.7	2.1	2.6
Bi	9.7	8.6	12.6	9.0	11.6	13.8	11.8	22.4	1.5	1.0	1.3	1.6	1.4	2.6
Th	152.3	122.1	95.0	106.4	100.8	96.5	68.8	95.8	0.8	0.9	0.8	0.8	0.6	0.8
U	71.2	61.4	49.8	49.4	52.0	49.2	44.2	49.8	0.8	0.8	0.8	0.8	0.7	0.8
Particle N	15.0	14.8	9.4	17.2	15.9	10.6	5.6	4.1	0.6	1.2	1.1	0.7	0.4	0.3
Particle M	583	507	238	557	387	192	125	216	0.5	1.1	0.8	0.4	0.2	0.4
V EF	2.8	2.6	3.0	3.0	2.9	3.1	2.7	2.8	1.1	1.2	1.1	1.2	1.0	1.1
Cr EF	3.6	3.2	3.6	3.9	3.6	3.6	3.3	3.7	1.1	1.2	1.1	1.1	1.0	1.1
Mn EF	5.2	4.9	4.7	4.9	5.1	5.3	4.0	4.4	1.0	1.0	1.0	1.1	0.8	0.9
Co EF	3.6	3.5	3.7	4.0	3.8	4.0	3.3	3.5	1.0	1.1	1.1	1.1	0.9	1.0
Ni EF	6.1	5.9	6.3	6.6	6.3	6.7	6.0	6.1	1.1	1.1	1.1	1.1	1.0	1.0
Cu EF	7.4	7.3	8.5	8.0	8.3	9.3	8.0	8.3	1.2	1.1	1.1	1.3	1.1	1.1
As EF	21.8	21.5	26.8	24.4	27.9	29.3	27.3	25.5	1.2	1.1	1.3	1.4	1.3	1.2
Rb EF	1.4	1.4	1.4	1.5	1.4	1.4	1.2	1.3	1.0	1.1	1.0	1.0	0.9	0.9
Sr EF	4.4	4.1	3.1	3.3	3.6	3.1	3.2	2.3	0.8	0.8	0.9	0.8	0.8	0.6
Mo EF	3.0	2.9	2.9	2.6	3.0	3.0	3.2	2.9	1.0	0.9	1.1	1.0	1.1	1.0
Cd EF	10.7	11.3	32.3	17.8	31.8	39.1	31.2	37.4	2.9	1.6	2.8	3.5	2.8	3.3
Sn EF	0.8	0.8	1.5	1.3	1.5	1.4	1.9	1.7	1.8	1.6	1.8	1.7	2.3	2.1
Sb EF	8.7	9.1	18.3	14.6	17.8	20.5	19.7	17.3	2.0	1.6	2.0	2.3	2.2	1.9
Tl EF	1.6	1.5	2.0	1.7	1.9	2.0	2.0	2.5	1.3	1.1	1.3	1.3	1.3	1.7
Pb EF	4.1	4.5	11.2	6.8	10.8	13.0	11.7	12.5	2.5	1.5	2.4	2.9	2.6	2.8
Bi EF	10.6	10.4	16.2	11.7	15.6	17.6	17.6	25.3	1.6	1.1	1.5	1.7	1.7	2.4
Th EF	1.9	1.8	1.5	1.7	1.8	1.5	1.2	1.4	0.8	0.9	1.0	0.8	0.7	0.8
U EF	3.8	3.6	3.3	3.5	3.4	3.3	3.2	2.8	0.9	1.0	0.9	0.9	0.9	0.8

[a]Trace element concentrations unit of measure is pg g^{-1}, the data of particle number unit of measure is 10^3/mL, and mass unit of measure is ppb g^{-1}. EF is enrichment factors and IF is increase factor. IF is calculated relative to element median concentrations pre-1953 AD.

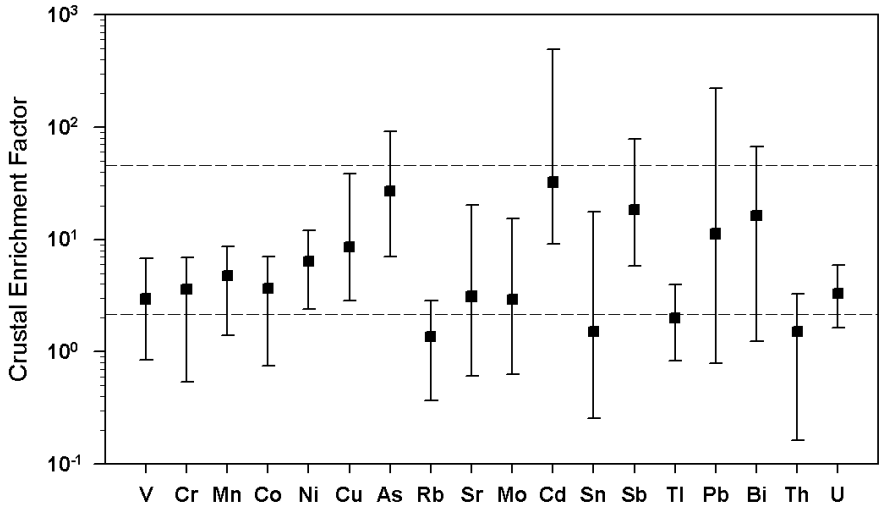

Figure 4. Median crustal enrichment factors (EF_c) for the measured trace elements of the Miaoergou ice core samples. The bars show the ranges of EF_c values, on a logarithmic *y* scale.

way, recent variations in trace elements can be considered within the framework of a longer historical context.

[18] Medians of post-1953 AD concentrations show little variation for Ba, V, Cr, Mn, Co, Ni, Cu, As, Rb, Mo, Th, and U and slight decrease for Sr (Table 3 and Figure 3). The most notable increases since 1953 AD are shown for Cd, Sn, Sb, Tl, Pb, and Bi, with different enrichment magnitudes and temporal trends (Table 3 and Figure 3). Generally, a slight increase occurred in 1950s for these elements, while a notable increase in 1960s. Cd and Pb concentrations show peaks in 1970s (Table 3). However, Tl, Sn, and Bi show peaks in 1990s and Sb shows a peak in 1980s.

[19] Figure 4 shows that EF_c values are highly variable, from one element to another and from one sample to another, highlighting the large variability in the importance of rock and soil dust contributions. Median EF_c values during the period 1953–2004 AD are less than 10 for V, Cr, Mn, Co, Ni, Cu, Rb, Sr, Mo, Sn, Tl, Th and U, and no significant increases are observed except for Sn and Tl (Table 3 and Figure 3). This implies that these elements originate mainly from rock and soil dust. In contrast, the high median EF_c values, with a range from 11.2 to 32.3 and increasing trends since 1953 AD are observed for Cd, Sb, Pb, and Bi (Table 3 and Figure 3), imply that contributions from anthropogenic sources might be important for these particular elements. High EF_c of As throughout the period 1953–2004 AD, together with a slight increase of EF_c in comparison to its pre-1953 AD level, suggests that As may have additional natural or anthropogenic inputs. For Sn and Tl, the EF_c values representing relatively low levels show an increase since ~1980s, probably due to an anthropogenic contribution.

3.3. Comparison With Other Data, in Terms of Concentrations and Fallout Fluxes of Trace Elements

[20] The results described here have been compared with those of ice samples from central Asia, i.e., Inilchek in central Tien Shan, Muztagh Ata in eastern Pamirs, and Mt. Qomolangma (Everest) in central Himalayas (Table 4). Since the trace element concentrations could be dependent upon accumulation rates, the fallout fluxes of trace elements were calculated, as presented in Table 4.

[21] All the Miaoergou, Inilchek, and Muztagh Ata locations (Figure 1) are surrounded by large desert regions. It is

Table 4. Comparisons of the Miaoergou Trace Element Concentrations (pg g^{-1}) and Fallout Fluxes (pg g^{-1} cm^{-2} yr^{-1}) With Other Remote Sites in Central Asia[a]

Site	Miaoergou	Inilchek[b]	Muztagh Ata[c]	Qomolangma[d]
Time period	1953–2004	1992–1998	1950–2000	1950–2002
Accumulation rate[e]	26	62	56	52
Coordinates	43°N, 94°′E	42°′N, 80°E	38°N, 75°E	28°N, 86°E
Altitude (m)	4512	5100	7010	6518
	Median	Median	Median	Median
Ba	4047		1600	344
V	934	801		97
Cr	734	958		95
Mn	15,014	6871	6200	1745
Co	247	2284		36
Rb	878		230	
Sr	5848		2600	371
Sb	35.3		9	
Tl	8.9			1.7
Bi	12.6		6	5.4
U	49.8			19
Ba fallout flux	10,5230		89,600	17,888
V fallout flux	24,284	49,662		5044
Cr fallout flux	19,079	59,396		4940
Mn fallout flux	390,353	426,002	347,200	90,740
Co fallout flux	6414	141,608		1872
Rb fallout flux	22,831		12,880	
Sr fallout flux	152,043		145,600	19,292
Sb fallout flux	918		504	
Tl fallout flux	231			88
Bi fallout flux	328		336	281
U fallout flux	1294			988

[a]Trace element concentrations unit of measure is pg g^{-1} and fallout fluxes unit of measure is pg g^{-1} cm^{-2} yr^{-1}.
[b]*Kreutz and Sholkovitz* [2000].
[c]*Y. Li et al.* [2006].
[d]*Kaspari et al.* [2009].
[e]Unit of measure is g H_2O cm^{-2} yr^{-1}.

shown that median concentrations of available elements (V, Cr, and Mn) at Inilchek are comparable with those at Miaoergou during the period 1992–1998 AD; however, fallout fluxes are lower at Miaoergou. On the other hand, median concentration and fallout flux of Co at Miaoergou are significantly lower than those at Inilchek. Such a difference occurs, possibly and partially because of differences in trace element analytical methods between sites. For example, the trace element samples were digested completely at Inilchek [*Kreutz and Sholkovitz*, 2000], whereas the Miaoergou samples were acidified by HNO_3 to 1% prior to analysis. Thus the trace element concentrations reported at Inilchek are representative of total (soluble and insoluble) element concentrations, while concentrations reported for Miaoergou, Muztagh Ata [*Y. Li et al.*, 2006], and Qomolangma [*Kaspari et al.*, 2009] are representative of the soluble, together with a portion of the insoluble element concentrations. Median concentrations of trace elements at Miaoergou are higher than those at Muztag Ata (7010 m a.s.l), but the fallout fluxes are at similar levels in spite of their different altitudes. Median concentrations and fallout fluxes of most of the trace elements at Miaoergou are over a magnitude higher than those at Qomolangma, indicating a larger dust contribution at Miaoergou.

3.4. Potential Source Regions for Trace Elements in the Miaoergou Area, as Indicated by Air Mass Trajectories

[22] Air-backward trajectories allow a hint about the potential source regions, where trace elements are emitted. Here, the Hybird Single-Particle Lagrangian Integrated Trajectory model (HYSPLIT 4.8) [*Draxler and Hess*, 1998] was adopted, to investigate the transport pathways of the aerosol particles. Five day backward trajectories, with a daily resolution to simulate the routes of air masses reaching the sampling site, were calculated for the period 1953–2004 AD. The clustering tool integrated into the model was applied to form clusters (mean backward trajectories) of all the trajectories for each year. Generally, two to four clusters for each year could be derived from the HYSPLIT model.

[23] The results indicate that westerlies prevail high over the Miaoergou area, with the air mass influxes originating from west, northwest, and north. For example, air trajectories in 1975 AD originated from several regions (Figure 5). Clusters represent air masses originating from west Russia (cluster 1), the eastern Mediterranean Sea and the Black Sea (cluster 2), the Atlantic Ocean (cluster 3), and the Caspian and Aral Seas (cluster 4). Air masses pass over the Caspian-Aral basin and Pamir Plateau and many countries and regions, such as Russian, Kazakhstan, Kyrgyzstan, Uzbekistan, Turkmenistan, and northwestern Xinjiang (China). The sources of the air masses, as revealed by air-backward trajectories, are consistent with the results based upon analysis of atmospheric circulation patterns during the period 1940–1991 AD over the Tien Shan, with three different moisture transport regimes (Atlantic, Arctic, Mediterranean) [*Aizen et al.*, 2006]. Thus it is possible that the Miaoergou ice may preserve both global and regional records of trace elements. Along the trajectories, there are large arid regions in central Asia and countries of the Commonwealth of Independent States (CIS) (Figure 1). When the air currents pass through these regions, aerosol particles can be entrained into the atmosphere and transport aloft for a long distance, especially for the fine particles, before being scavenged by dry and wet deposition in Tien Shan. The long-range transport of pollutants within aerosol particles results in the deposition and enrichment of trace elements in the Miaoergou ice, far from the source regions. The countries in Eurasia covered by the westerly wind path, particularly Russia, central Asian CIS (Tajikistan, Kyrgyzstan, Kazakhstan, Turkmenistan, and Uzbekistan) and northwestern Xinjiang of China, which are located in the nearest upwind regions of the Miaoergou area, are considered to be the main source regions for trace elements.

3.5. Relationship Between Crustal Origin Elements and Atmospheric Dust Inputs

[24] As discussed above, the increasing trends in median concentrations and EF_c of most of the elements during the period 1953–2004 AD relative to the pre-1953 AD levels are insignificant (Table 3). Among these elements, median concentrations of Ba, Mn, Rb, Th, and U decreased slightly, while the most notable decrease is shown for Sr. In case of the decrease of accumulation rate during recent decades in the Miaoergou glacier, there are more significant decreases in the fallout fluxes of these elements. The decreases of crustal origin elements may be attributed to a change of dust loading in the atmosphere and hence dust deposition during recent decades in the Tien Shan region.

[25] It is suggested that the snow and ice chemistry in Tien Shan is dominated by desert dust, originating from the surrounding wide arid and semiarid regions [*Wake et al.*, 1990]. High-frequency dust storms generated in West China and its surrounding regions, during winter and spring, play an important role in the atmospheric dust loading over the region. A reconstructed long-term record of dust storms in northern China indicates that the frequencies of dust storms decreased twofold from 1950s through 1970s to the mid-1980s [*Qian et al.*, 2002]. The dust storm activity exhibited a significant decreasing trend (~2 times) during the past ~50 years, over the Tibetan Plateau. This is indicated by the insoluble particle record of an ice core from Mt. Qomolangma [*Xu et al.*, 2007]. An approximately threefold decrease in dust concentrations in mid-1970s was also observed in the soluble dust ion records from Mt. Geladaindong, Tibetan Plateau [*Grigholm et al.*, 2009]. The decreasing trend of dust loading in the surrounding regions of Tien Shan may result from increasing precipitation during recent decades in the source regions, such as the semiarid region in northern China [*Wang and Li*, 1990], continental Asia [*Aizen et al.*, 2001], and northern Eurasia [*Wang and Cho*, 1997], including western Siberia, northern and western regions of Tien Shan, and Pamir. Although annual precipitation showed an increasing trend over the region, this could not compensate for the mass loss (decrease accumulation rate) since 1970s in the Miaoergou glacier and glaciers in eastern Tien Shan, due to summer temperature increase during recent decades in the region [*Z. Li et al.*, 2007b; *Wang et al.*, 2009]. The decrease in wind speed during recent decades, related to late 20th century climate warming over Asia, is also a potentially important mechanism for the decreasing trend of dust storms over the region [*Grigholm et al.*, 2009]. In addition, it is suggested that an increase in precipitation, glacial meltwater, river runoff, and temperature, during recent decades in northwestern China, resulted in enhanced vegetation cover

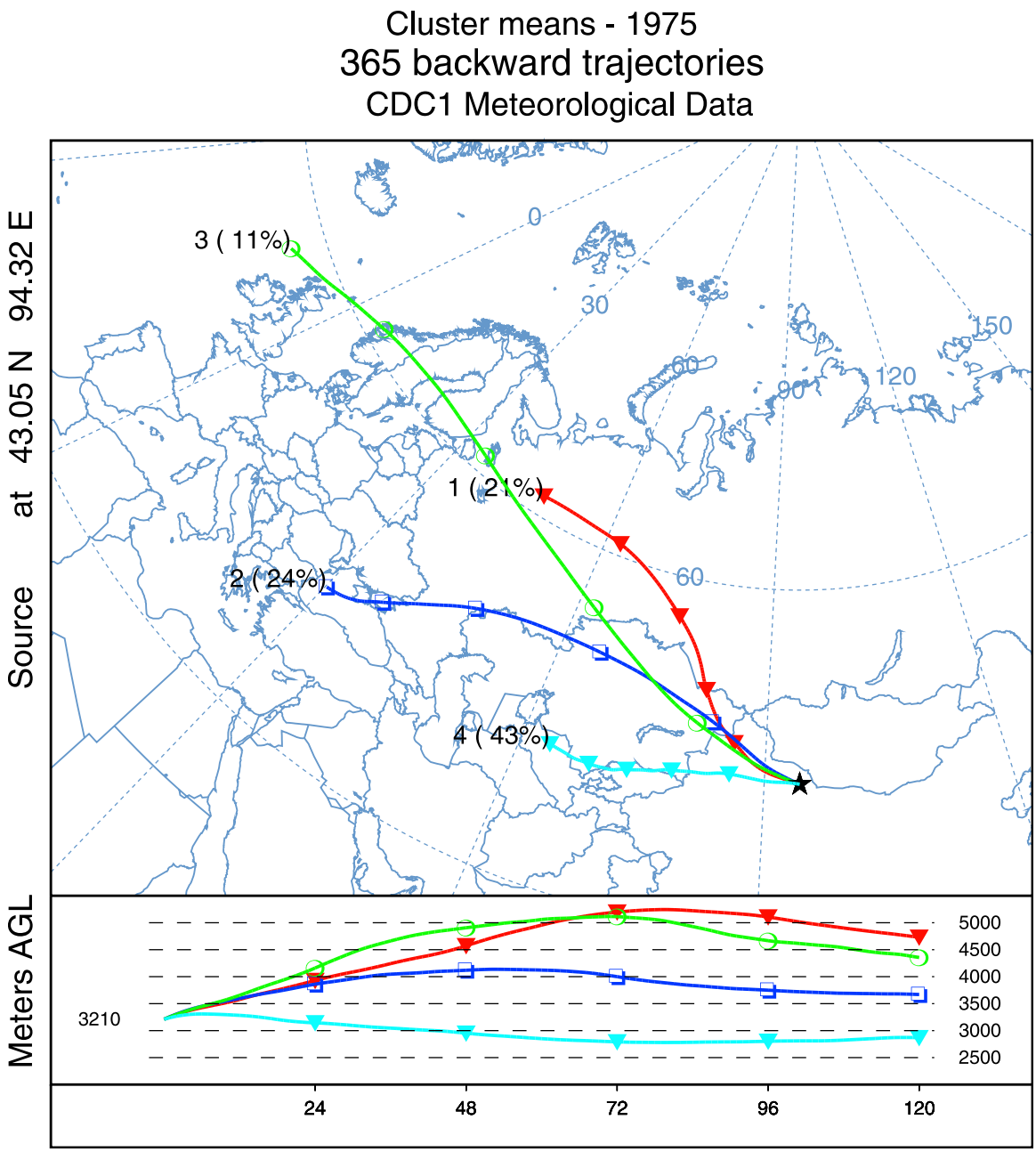

Figure 5. Mean 5 day backward air trajectories reaching the Miaoergou ice core drilling site in 1975 AD, simulated by the HYSPLIT 4.8 model. The altitude (3210 m a.s.l.) represents meter above ground level (AGL). The serial number and relative percentage of trajectories for each cluster are given.

and a reduction in the number of days with sand-dust storms [*Shi et al.*, 2007]. Such results can be verified further by investigating the dust record related to the same ice core. Median insoluble particle numbers and mass concentrations (or fallout fluxes) have decreased significantly since 1953 AD (Table 3), indicating that dust concentrations in 1990s are only half of those in 1950s and 1960s.

3.6. Contributions From Anthropogenic Sources

[26] In the emission inventory of trace elements to the atmosphere, major anthropogenic sources include fossil fuel combustion, gasoline combustion, nonferrous metal production, operation in ferrous foundries, refuse incineration, and cement production [*Pacyna and Pacyna*, 2001]. However, it should be pointed out that emission inventory available, for anthropogenic sources of trace elements, provides an overview on a global scale. This pattern can be entirely different when considered on a local/regional scale [*Pacyna and Pacyna*, 2001]. Here, we focus upon investigating the anthropogenic sources and the spatial extent of the 20th century enrichment of elements for which anthropogenic contributions are important, including Sb, Bi, Pb, Cd, Tl, and Sn.

3.6.1. Antimony

[27] Potential anthropogenic sources of Sb emission, to the atmosphere, include coal combustion, lead and copper smelting, refuse burning, and various end uses [*Pacyna and Pacyna*, 2001; *Krachler et al.*, 2005b]. Although China has been the country with the largest emission of Sb in the world since 1990s, most Sb ores and mining and smelting activities of Sb are distributed in southern China [*Zhang*, 1998], far away from potential source regions of Sb in the Miaoergou ice. Hence it is only anthropogenic emissions of Sb from the countries within the source regions that are believed to dominate Sb emissions. Prior to 1995 AD, Kyrgyzstan was the leading producer of Sb in the CIS, with a steady increase of Sb production from 1950s to 1990s. Afterward, Sb production declined sharply due to a reduction in the supply of raw materials of Sb [*Y. Li et al.*, 2006, and references therein]. Russia has become an important producer of Sb in the world during recent years [*Krachler et al.*, 2005b]. In addition, the coal combustion for heat supply and electricity generation which has been widely used in many countries in the source regions might be another important source for Sb emissions in the area.

[28] Sb concentrations in the Miaoergou ice began to increase in 1950s, peaking in 1980s. Since then, Sb concentrations declined throughout the period 1990–2004 AD. This is likely to be related to a reduction in Sb production in the source region during recent years (e.g., Kyrgyzstan). Similar to the Miaoergou time series, Sb concentrations in the Muztagh Ata ice core from the Pamirs showed an increasing trend from 1950s to the beginning of 1990s [*Y. Li et al.*, 2006]. Afterward, Sb concentrations decreased. Increased Sb concentrations during the second half of the 20th century, relative to preindustrial levels, are also observed in snow from Monte Rosa, European Alps [*Barbante et al.*, 2004]. In contrast, Sb concentrations reached a maximum value in late 1950s in the firn core from the Devon ice cap, Arctic Canada and, since then, Sb concentrations have declined [*Krachler et al.*, 2005b]. This pattern suggests that increase in atmospheric Sb is widespread in the Northern Hemisphere, but periods of peak concentrations vary between sites, resulting from difference in geographical locations, rise and fall of Sb emissions in the relevant source regions. Chronologically reliable records of changes in Sb concentrations in Antarctic snow and ice are not available. Such data are required to assess the anthropogenic influence on the atmospheric Sb cycle on a global scale.

3.6.2. Bismuth

[29] To the knowledge of the authors, there is no published inventory of anthropogenic emissions of Bi to the atmosphere. Potential anthropogenic sources of Bi emission include refuse burning, silver and lead mining and smelting, and fossil fuel combustion [*Ferrari et al.*, 2000]. Kazakhstan and Russia, within the source regions, are major producers of Bi [*Brown*, 2000].

[30] Bi concentrations in the Miaoergou ice began to increase in 1960s and showed a notable increase in 1970s. This was followed by a slight decline in 1980s, reaching a maximum during the period 1990–2004 AD. Global Bi production peaked in 1970s, with Northern Hemisphere production peaking from 1970s to 1990s [*Kaspari et al.*, 2009]. Increases in Bi concentrations and EF_c within the second half of the 20th century are also documented in the Muztagh Ata ice core [*Y. Li et al.*, 2006] and the Qomolangma ice core [*Kaspari et al.*, 2009], with a peak in 1990s. Although no significant trend is observed in Bi concentrations in snow from Summit, Greenland, during the period 1967–2002 AD, the Bi/Al ratio increased ~6 times, relative to its natural Holocene values, which has been attributed to anthropogenic emissions [*Ferrari et al.*, 2000]. Continuous increases in concentrations and EF_c of Bi were also observed in Antarctic snow from Coats Land during the period 1960s to 1990s [*Planchon et al.*, 2002]. All data available from other locations including our data provide unequivocal evidence that human influences are currently the dominant factor controlling atmospheric cycle of Bi on a global scale.

3.6.3. Lead

[31] The combustion of leaded, low-leaded, and unleaded gasoline is the major source of atmospheric Pb emission on a global scale [*Pacyna and Pacyna*, 2001] and over the territory of CIS [*Kakareka et al.*, 2004], which is a potential source region of the Miaoergou Pb records. Other major anthropogenic sources include emissions from nonferrous metal production, steel making, coal burning, and refuse incineration [*Pacyna and Pacyna*, 2001; *Kakareka et al.*, 2004]. Russia and Kazakhstan are likely to be the important source countries for Pb in the Miaoergou ice, since they are the two largest countries that release anthropogenic Pb into the atmosphere in the CIS region [*Kakareka et al.*, 2004]. In addition, Ürümqi city in Xinjiang (Figure 1), China, which is located upwind of Miaoergou, is expected to be an important local source of Pb due to its large number of automobiles and wide use of coal-burning, for energy supply.

[32] Detailed investigations in the northern hemisphere have documented a comprehensive time course for changes in Pb concentrations in snow and ice from Greenland [*Boutron et al.*, 1991; *Hong et al.*, 1994; *Candelone et al.*, 1995; *McConnell et al.*, 2002; *McConnell and Edwards*, 2008], the European Alps [*Schwikowski et al.*, 2004], Muztagh Ata [*Z. Li et al.*, 2006], Canadian Arctic [*Zheng et al.*, 2007], and the Antarctic [*Wolff and Suttie*, 1994; *Vallelonga et al.*, 2002; *Planchon et al.*, 2003]. The Greenland records have provided two major large-scale Pb pollution events in the Northern Hemisphere, an early large-scale pollution two millennia ago due to Pb and Ag mining and smelting activities and, more recently, the highest level of Pb occurring during 1960s, linked to the extensive use of Pb additives in gasoline since 1930s. The Antarctic records displayed that the first influence of atmospheric Pb took place from the late 19th to the early 20th centuries due to Pb mining and smelting in Australia and the second massive Pb pollution occurred from 1960s to 1980s, in association with the vast use of Pb additives in gasoline in the Southern Hemisphere.

[33] By comparison, snow and ice records from the other locations close to the source regions show different input patterns of Pb pollutants likely due to different geographical characteristics and sources. Our record shows that a significant anthropogenic influence is not detectable before the second half of the 20th century and the first major Pb enhancement occurred during the 1970s. A similar Pb peak during the same time period was observed in the ice from the Monte Rosa in the Alps.

[34] These observations suggest that enrichment of Pb is widespread, but input time varies regionally. Interestingly, the recent Miaoergou Pb concentrations are higher than those observed in 1980s. This increase in concentrations is attributed probably to the continuous use of leaded gasoline until 2000 AD and an increase in the number of motor vehicles during recent years, in upwind source countries and areas such as central Asian CIS [*Z. Li et al.*, 2006] and Xinjiang, China. Moreover, an increase in demand for electricity and heat by means of combustion of fossil fuels, particularly coal, has been also observed in many countries during recent years, particularly in Asia [*Pacyna and Pacyna*, 2001].

3.6.4. Cadmium

[35] The worldwide potential anthropogenic sources of Cd emissions to the atmosphere include various human activities such as metal production, combustion of fossil fuels, and other industrial processes [*Pacyna and Pacyna*, 2001]. Russia, Uzbekistan, and Kazakhstan could be important source countries, with their large emission of Cd to atmosphere [*Kakareka et al.*, 2004]. However, local sources (e.g., Xinjiang) of Cd are not clear, due to the absence of emission data.

[36] Increased Cd concentrations during the second half of the 20th century, compared with preindustrial levels, are also observed in snow and ice from Greenland [*Candelone et al.*, 1995; *McConnell and Edwards*, 2008] and the European Alps [*Barbante et al.*, 2004]. However, no significant increase in Cd concentration is observed in snow from Coats Land, Antarctica [*Planchon et al.*, 2002]. The Miaoergou temporal trend of Cd concentrations is similar to this pattern, with Cd peaking in 1970s, followed by a slight decline in 1980s and an increase again during the period 1990–2004 AD. This trend differs from the Greenland and European Alps records, which show peak concentrations in 1960s and 1970s, respectively. After this, Cd concentrations decrease slowly during recent decades, due to the control of industrial emissions in the northern hemisphere such as Europe and North America [*Candelone et al.*, 1995; *Barbante et al.*, 2004; *McConnell and Edwards*, 2008]. The recent increase in the Miaoergou Cd concentrations could be explained by an increasing trend of Cd emission, resulting from the growing demands for energy and increasing industrial production, together with less efficient emission control in Asia [*Pacyna and Pacyna*, 2001].

3.6.5. Thallium

[37] Tl concentrations remained relatively constant during the second half of the 20th century, while elevated EF_c values are observed since 1990s (Table 3). Considering the decreased dust deposition during recent decades in Tien Shan region, this feature may indicate that anthropogenic Tl input compensated for the reduction of crustal Tl input, leading to less variable concentration levels with a prominent increasing trend of EF_c values during recent decades. Pronounced increases of Tl concentrations starting in the middle of the 19th century were observed in Greenland ice core [*McConnell and Edwards*, 2008] and an ice core from Illimani, Bolivia [*Kellerhals et al.*, 2010]. Such increases were attributed to an anthropogenic contribution mainly from coal burning. Coal for heat supply and electricity is extensively used in source regions in Asia [*Pacyna and Pacyna*, 2001]. It is therefore plausible from our ice core record that anthropogenic Tl derived from coal combustion has dominated the atmospheric deposition of Tl in the Tien Shan during recent decades. This suggests that anthropogenic influence on the atmospheric cycle of Tl is widespread. Reliable comprehensive snow and ice records of changes in Tl in Antarctica will be helpful to understand that anthropogenic contamination by Tl has become a global problem reaching even the most remote areas.

3.6.6. Tin

[38] Finally, the slight increase in concentrations and more elevation of EF_c values for Sn are also observed during recent decades (Table 3), suggesting that anthropogenic Sn input is probably important. Such an attribution was also observed in the Qomolangma ice core, resulting largely from stationary fossil fuel combustion and nonferrous metals production [*Hong et al.*, 2009]. It is, however, important to note that little is known about long-term trends of Sn to understand the extent and course of anthropogenic perturbation of atmospheric Sn cycle. More comprehensive time series from snow and ice cores in both hemispheres would provide detailed information on temporal and spatial changes in atmospheric composition, in response to emissions of Sn by different anthropogenic activities and from different source regions.

4. Summary and Conclusions

[39] This study provides the first high-resolution records of 19 trace elements in the high-altitude Miaoergou ice core, from eastern Tien Shan, during the period 1953–2004 AD. Significant seasonal variations in the concentrations of trace elements are observed. The records show contrasting temporal trends for different elements during the second half of the 20th century, with comparison to that of pre-1953 AD.

[40] The source regions and the contributions of atmospheric pathways to the trace element records are investigated by the HYSPLIT 4.8 model, indicating that the Miaoergou ice preserves mainly local and regional atmospheric chemical records. Potential source regions are located in vast areas of the Eurasia territories covered by the westerly wind path, particularly in northwestern Xinjiang (China), Russia, and central Asian CIS countries.

[41] It is suggested that decreased Ba, Mn, Rb, Th, U, and Sr concentrations (or fallout fluxes) along the Miaoergou ice core result from declines in atmospheric dust inputs and accumulation rate during recent decades. The rock and soil dust is the most important natural source for most of the elements. However, anthropogenic emissions have been influencing the atmospheric cycles of the enrichments of Cd, Sb, Pb, Bi, Tl, and Sn during recent decades. Potential anthropogenic sources for these elements include metal smelting, mining, stationary fossil fuel combustion, and combustion of gasoline. The enrichments of Pb and Bi, during the second half of 20th century, are also documented at other remote sites even including Antarctica. This suggests that the increase in these elements, within the atmosphere, is widespread on a global scale. For Cd, no pollution signals were observed in Antarctica, leading to an assessment that Cd is an element polluting the atmosphere on a large scale, but a global dispersion is still limited for this element. For Sb, Tl, and Sn, our data support regional signals of atmospheric pollution previously observed in very confined locations. However, more detailed time series from

snow and ice cores in other remote locations in both hemispheres will be necessary to accurately evaluate the role of anthropogenic activities affecting the dispersion and perturbation of their atmospheric geochemical cycles on a global scope. For all elements, the differences in the periods of peaks between sites are attributed to differences in locations and element sources.

[42] **Acknowledgments.** This research was funded by the National Basic Research program of China (2010CB951401; 2007CB411501), Natural Science Foundation of China (40825017), the Chinese Academy of Sciences (SKLCS-ZZ-2008-06), and the Nanjing University. In Korea, this work was supported by KOPRI research grant (PP09010) and INHA University Research grant (INHA-40890-01). We greatly appreciate the comments from Michael Collins, Zhang Zhiyi, Paul A. Mayewski, Bjorn Grigholm, Jo Jacka, and anonymous reviewers for the improvement of our paper and all field personnel for the scientific expedition to the Miaoergou glacier in 2005.

References

Aizen, E. M., V. B. Aizen, J. M. Melack, T. Nakamura, and T. Ohta (2001), Precipitation and atmospheric circulation patterns at mid-latitudes of Asia, *Int. J. Climatol.*, *21*, 535–556, doi:10.1002/joc.626.

Aizen, V. B., E. M. Aizen, D. Joswiak, K. Fujita, N. Takeuchi, and S. Nikitin (2006), Climatic and atmospheric circulation pattern variability from ice-core isotope/geochemistry records (Altai, Tien Shan and Tibet), *Ann. Glaciol.*, *43*, 49–60, doi:10.3189/172756406781812078.

Araguás-Araguás, L., K. Froehlich, and K. Rozanski (1998), Stable isotopic composition of precipitation over southeast Asia, *J. Geophys. Res.*, *103*(D22), 28,721–28,742, doi:10.1029/98JD02582.

Barbante, C., et al. (2004), Historical record of European emissions of trace elements to the atmosphere since the 1650s from alpine snow/ice cores drilled near Monte Rosa, *Environ. Sci. Technol.*, *38*(15), 4085–4090, doi:10.1021/es049759r.

Boutron, C. F., U. Görlach, J. P. Candelone, M. A. Bolshov, and R. J. Delmas (1991), Decrease in anthropogenic lead, cadmium and zinc in Greenland snows since the late 1960s, *Nature*, *353*, 153–156, doi:10.1038/353153a0.

Boutron, C. F., J. P. Candelone, and S. Hong (1995), Greenland snow and ice cores: Unique archives of large-scale pollution of the troposphere of the Northern Hemisphere by lead and other heavy metals, *Sci. Total Environ.*, *160–161*, 233–241, doi:10.1016/0048-9697(95)04359-9.

Brown, R. D. (2000), Bismuth, in *U. S. Geological Survey Minerals Yearbook*, pp. 131–134, U. S. Geol. Surv., Reston, Va.

Candelone, J. P., S. Hong, and C. F. Boutron (1994), An improved method for decontaminating polar snow or ice cores for heavy metal analysis, *Anal. Chim. Acta*, *299*, 9–16, doi:10.1016/0003-2670(94)00327-0.

Candelone, J. P., S. Hong, C. Pellone, and C. F. Boutron (1995), Post-industrial Revolution changes in large scale atmospheric pollution of the Northern Hemisphere for trace elements as documented in central Greenland snow and ice, *J. Geophys. Res.*, *100*(D8), 16,605–16,616, doi:10.1029/95JD00989.

Draxler, R. R., and G. D. Hess (1998), An overview of the HYSPLIT-4 modeling system for trajectories, dispersion, and deposition, *Aust. Meteorol. Mag.*, *47*, 295–308.

Ferrari, C. P., S. Hong, K. Van de Velde, C. F. Boutron, S. N. Rudniev, M. Bolshov, W. Chisholm, and K. J. R. Rosman (2000), Natural and anthropogenic bismuth in central Greenland, *Atmos. Environ.*, *34*(6), 941–948, doi:10.1016/S1352-2310(99)00257-5.

Grigholm, B., P. Mayewski, S. Kang, Y. Zhang, S. Kaspari, S. Sneed, and Q. Zhang (2009), Atmospheric soluble dust records from a Tibetan ice core: Possible climate proxies and teleconnection with the Pacific Decadal Oscillation, *J. Geophys. Res.*, *114*, D20118, doi:10.1029/2008JD011242.

Hong, S., J. P. Candelone, C. C. Patterson, and C. F. Boutron (1994), Greenland ice evidence of hemispheric scale pollution for lead two millennia ago by Greek and Roman civilizations, *Science*, *265*, 1841–1843, doi:10.1126/science.265.5180.1841.

Hong, S., C. Barbante, C. F. Boutron, P. Gabrielli, V. Gaspari, P. Cescon, L. Thompson, C. Ferrari, B. Francou, and L. Maurice-Bourgoin (2004), Atmospheric heavy metals in tropical South America during the past 22,000 years recorded in a high altitude ice core from Sajama, Bolivia, *J. Environ. Monit.*, *6*, 322–326, doi:10.1039/b314251e.

Hong, S., K. Lee, S. Hou, S. D. Hur, J. Ren, L. Burn, K. J. R. Rosman, C. Barbante, and C. Boutron (2009), An 800-year record of atmospheric As, Mo, Sn, and Sb deposition in central Asia in high-altitude ice cores from Mt. Qomolangma (Everest), Himalayas, *Environ. Sci. Technol.*, *43*(21), 8060–8065, doi:10.1021/es901685u.

Hou, S., D. Qin, P. Mayewski, Q. Yang, J. Ren, Z. Li, and C. Xiao (1999), Climatological significance of $\delta^{18}O$ in precipitation and ice cores: A case study at the head of Urumqi River, Tien Shan, China, *J. Glaciol.*, *45*(151), 517–523.

Kakareka, S., S. Gromov, J. Pacyna, and T. Kukharchyk (2004), Estimation of heavy metal emission fluxes on the territory of the NIS, *Atmos. Environ.*, *38*, 7101–7109, doi:10.1016/j.atmosenv.2004.03.079.

Kaspari, S., P. Mayewski, M. Handley, E. Osterberg, S. Kang, S. Sneed, S. Hou, and D. Qin (2009), Recent increases in atmospheric concentrations of Bi, U, Cs, S, and Ca from a 350-year Mount Everest ice core record, *J. Geophys. Res.*, *114*, D04302, doi:10.1029/2008JD011088.

Kellerhals, T., L. Tobler, S. Brütsch, M. Sigl, L. Wacker, H. W. Gäggeler, and M. Schwikowski (2010), Thallium as a tracer for pre-industrial volcanic eruptions in an ice core record from Illimani, Bolivia, *Environ. Sci. Technol.*, *44*, 888–893, doi:10.1021/es902492n.

Krachler, M., J. Zheng, D. Fisher, and W. Shotyk (2005a), Analytical procedures for improved trace element detection limit in polar ice from Arctic Canada using ICP-SMS, *Anal. Chim. Acta*, *530*, 291–298, doi:10.1016/j.aca.2004.09.024.

Krachler, M., J. Zheng, R. Koerner, C. Zdanowicz, D. Fisher, and W. Shotyk (2005b), Increasing atmospheric antimony contamination in the northern hemisphere: Snow and ice evidence from Devon Island, Arctic Canada, *J. Environ. Monit.*, *7*, 1169–1176, doi:10.1039/b509373b.

Kreutz, K. J., and E. R. Sholkovitz (2000), Major elements, rare earth element, and sulfur isotopic composition of a high-elevation firn core: Sources and transport of mineral dust in central Asia, *Geochem. Geophys. Geosyst.*, *1*(11), 1048, doi:10.1029/2000GC000082.

Lee, K., S. D. Hur, S. Hou, S. Hong, X. Qin, J. Ren, Y. Liu, K. J. R. Rosman, C. Barbante, and C. F. Boutron (2008), Atmospheric pollution for trace elements in the remote high-altitude atmosphere in central Asia as recorded in snow from Mt. Qomolangma (Everest) of the Himalayas, *Sci. Total Environ.*, *404*, 171–181, doi:10.1016/j.scitotenv.2008.06.022.

Li, Y., T. Yao, N. Wang, Z. Li, L. Tian, B. Xu, and G. Wu (2006), Recent changes of atmospheric heavy metals in a high elevation ice core from Muztagh Ata in East Pamirs: Initial results, *Ann. Glaciol.*, *43*, 154–159, doi:10.3189/172756406781812186.

Li, Y., T. Yao, Z. Li, Z. Li, Y. Liu, and J. Duan (2007), Determination of trace elements in snow and ice by double focusing inductively coupled plasma-mass spectrometry (in Chinese with English abstract), *Chin. J. Anal. Chem.*, *35*(1), 37–42.

Li, Z., T. Yao, L. Tian, B. Xu, and Y. Li (2006), Atmospheric Pb variations in central Asia since 1955 from Muztagh Ata ice core record, eastern Pamirs, *Chin. Sci. Bull.*, *51*(16), 1996–2000, doi:10.1007/s11434-006-2061-9.

Li, Z. Q., C. Li, Y. Li, F. Wang, and H. Li (2007a), Preliminary results from measurements of selected trace metals in the snow-firn pack on Ürümqi glacier No. 1, eastern Tien Shan, China, *J. Glaciol.*, *53*(182), 368–373, doi:10.3189/002214307783258486.

Li, Z. Q., F. Wang, G. Zhu, and H. Li (2007b), Basic features of the Miaoergou flat-topped glacier in East Tian Shan Mountains and its thickness change over the past 24 years (in Chinese with English abstract), *J. Glaciol. Geocryol.*, *29*(1), 61–65.

Liu, Y., S. Hou, and Y. Zhang (2009), The acid cleaning method of labware for trace element analysis in snow and ice samples, *Sci. Cold Arid Regions*, *1*(6), 0502–0508.

McConnell, J., and R. Edwards (2008), Coal burning leaves toxic heavy metal legacy in the Arctic, *Proc. Natl. Acad. Sci. U. S. A.*, *105*, 12,140–12,144, doi:10.1073/pnas.0803564105.

McConnell, J., G. Lamorey, and M. Hutterli (2002), A 250-year high-resolution record of Pb flux and crustal enrichment in central Greenland, *Geophys. Res. Lett.*, *29*(23), 2130, doi:10.1029/2002GL016016.

Pacyna, J. M., and E. G. Pacyna (2001), An assessment of global and regional emissions of trace metals to the atmosphere from anthropogenic sources worldwide, *Environ. Rev.*, *9*, 269–298, doi:10.1139/er-9-4-269.

Planchon, F. A. M., C. F. Boutron, C. Barbante, G. Cozzi, V. Gaspari, E. W. Wolff, C. P. Ferrari, and P. Cescon (2002), Changes in heavy metals in Antarctic snow from Coats Land since the mid-19th to the late-20th century, *Earth Planet. Sci. Lett.*, *200*, 207–222, doi:10.1016/S0012-821X(02)000612-X.

Planchon, F. A. M., K. Van de Velde, K. J. R. Rosman, E. Wolff, C. Ferrari, and C. Boutron (2003), One hundred fifty-year record of lead isotopes in Antarctic snow from Coats Land, *Geochim. Cosmochim. Acta*, *67*, 693–708, doi:10.1016/S0016-7037(02)01136-5.

Qian, W. H., L. S. Quan, and S. Y. Shi (2002), Variations of the dust storm in China and its climatic control, *J. Clim.*, *15*, 1216–1229, doi:10.1175/1520-0442(2002)015<1216:VOTDSI>2.0.CO;2.

Schwikowski, M., et al. (2004), Post-17th-century changes of European lead emissions recorded in high-altitude alpine snow and ice, *Environ. Sci. Technol.*, *38*(4), 957–964, doi:10.1021/es034715o.

Shi, Y., Y. Sheng, E. Kang, D. Li, Y. Ding, G. Zhang, and R. Hu (2007), Recent and future climate change in northwest China, *Clim. Change*, *80*, 379–393, doi:10.1007/s10584-006-9121-7.

Vallelonga, P., K. Van de Velde, J. P. Candelone, V. Morgan, C. Boutron, and K. J. R. Rosman (2002), The lead pollution history of Law Dome, Antarctica, from isotopic measurements on ice cores: 1500 AD to 1989AD, *Earth Planet. Sci. Lett.*, *204*, 291–306, doi:10.1016/S0012-821X(02)00983-4.

Van de Velde, K., C. Boutron, C. Ferrari, A. Moreau, R. Delmas, C. Barbante, T. Bellomi, G. Capodaglio, and P. Cescon (2000), A two hundred years record of atmospheric cadmium, copper and zinc concentrations in high altitude snow and ice from the French-Italian Alps, *J. Geophys. Res.*, *27*(2), 249–252, doi:10.1029/1999GL010786.

Wake, C. P., P. A. Mayewski, and M. J. Spencer (1990), A review of central Asian glaciochemical data, *Ann. Glaciol.*, *16*, 45–52.

Wang, W. C., and K. Li (1990), Precipitation fluctuation over semiarid region in northern China and the relationship with EI Nino/Southern Oscillation, *J. Clim.*, *3*(7), 769–783, doi:10.1175/1520-0442(1990)003<0769:PFOSRI>2.0.CO;2.

Wang, X. L., and H. R. Cho (1997), Spatial-temporal structures of trend and oscillatory variabilities of precipitation over Northern Eurasia, *J. Clim.*, *10*(9), 2285–2298, doi:10.1175/1520-0442(1997)010<2285:STSOTA>2.0.CO;2.

Wang, Y., S. Hou, and Y. Liu (2009), Glacier changes in the Karlik Shan, eastern Tien Shan, during 1971/72–2001/02, *Anal. Glaciol.*, *50*(53), 1–7.

Wedepohl, K. H. (1995), The composition of the continental crust, *Geochim. Cosmochim. Acta*, *59*(7), 1217–1232, doi:10.1016/0016-7037(95)00038-2.

Wolff, E. W., and E. D. Suttie (1994), Antarctic snow record of Southern Hemispheric lead pollution, *Geophys. Res. Lett.*, *21*, 781–784, doi:10.1029/94GL00656.

Xu, J., S. Hou, D. Qin, S. Kang, J. Ren, and J. Ming (2007), Dust storm activity over the Tibetan Plateau recorded by a shallow ice core from the north slope of Mt. Qomolangma (Everest), Tibet-Himal region, *Geophys. Res. Lett.*, *34*, L17504, doi:10.1029/2007GL030853.

Zhang, G. (1998), Types of Chinese antimony ore and temporary and spatial distribution (in Chinese with English abstract), *Mineral Geol.*, *12*(5), 306–311.

Zheng, J., W. Shotyk, M. Krachler, and D. Fisher (2007), A 15,800-year of atmospheric lead deposition on the Devon Island Ice Cap, Nunavut, Canada: Natural and anthropogenic enrichment, isotopic composition, and predominant sources, *Global Biogeochem. Cycles*, *21*, GB2027, doi:10.1029/2006GB002897.

S. Hong, S. D. Hur, and K. Lee, Korea Polar Research Institute, Incheon 406-840, South Korea.

S. Hou and Y. Liu, State Key Laboratory of Cryospheric Sciences, Cold and Arid Regions Environmental and Engineering Research Institute, Chinese Academy of Sciences, Lanzhou, 730000, China. (shugui@lzb.ac.cn)

Y. Wang, Shandong Marine Fisheries Research Institute, Yantai 264006, China.